Journal of Medicinal Chemistry

Article

F-labeled Benzyldiamine Derivatives as Novel Flexible Probes for Positron Emission Tomography of Cerebral #-amyloid Plaque

Zijing Li, Xuran Zhang, Xiaoyang Zhang, Mengchao Cui, Jie Lu, Xiaodong Pan, and Xianzhong Zhang

J. Med. Chem., **Just Accepted Manuscript** • Publication Date (Web): 15 Nov 2016

ACS Publications

Journal of Medicinal Chemistry is published by the American Chemical Society. 1155 Sixteenth Street N.W., Washington, DC 20036

^{18}F-labeled Benzyldiamine Derivatives as Novel Flexible Probes for Positron Emission Tomography of Cerebral *β*-amyloid Plaque

Zijing Li[*, †, ⊥], Xuran Zhang[†, ‡, ⊥], Xiaoyang Zhang[‡], Mengchao Cui[‡], Jie Lu[‡], Xiaodong Pan[*, §, ‖], and Xianzhong Zhang[*, †]

[†]Center for Molecular Imaging and Translational Medicine, State Key Laboratory of Molecular Vaccinology and Molecular Diagnostics, School of Public Health, Xiamen University, Xiamen, Fujian 361102, China.

[‡]Key Laboratory of Radiopharmaceuticals, Ministry of Education, College of Chemistry, Beijing Normal University, Beijing 100875, China.

[§]Department of Neurology and Geriatrics, Fujian Institute of Geriatrics, Fujian Medical University Union Hospital, Fuzhou 350001, China.

[‖]Key Laboratory of Brain Aging and Neurodegenerative Disease, Fujian Key Laboratory of Molecular Neurology, Fujian Medical University, Fuzhou 350001, China.

[⊥]These authors contributed equally to the work.

Abstract

Early noninvasive visualization of cerebral *β*-amyloid (A*β*) plaques with positron emission tomography (PET) is the most feasible way to diagnose Alzheimer's disease (AD). In this study, a series of flexible benzyldiamine derivatives (BDA) were proposed to bind to the aggregated *β*-amyloid 1-42 (A$\beta_{1\text{-}42}$) with high adaptability, high binding affinity to A$\beta_{1\text{-}42}$ (6.8

± 0.6 nM) and rapid body excretion. Methylthio derivative (**12**) and ethoxyl derivative (**10**) were further labeled with ^{18}F directly on their benzene ring and examined as PET probes for Aβ plaque imaging. [^{18}F]**12** displayed 4.87 ± 0.52 %ID/g initial uptake and prompt washout from normal brain in biodistribution. MicroPET-CT imaging of transgenic mice indicated sufficient retention but lower white matter uptake in the AD transgenetic mouse brain compared with commercial [^{18}F]AV-45. Our experimental results provide new hints for developing targeting ligands with flexible framework as efficient Aβ probes for PET of AD brain.

Keywords: benzyldiamine derivatives; Aβ plaques; Alzheimer's disease; PET imaging agent; flexible scaffold;

Introduction

Alzheimer's disease (AD), a widespread and devastating neurodegenerative disease, afflicts a large population of patients especially seniors.[1] The intricate symptoms of AD are considered to be irreversible,[2] therefore early diagnosis as the foundation of the timely interference is extremely crucial. However, relying on the indirect examination of subsequent deterioration of mental or cognitive status, traditional clinical diagnosis of AD does not reflect the early onset neuropathological characteristics[3] Tau hypothesis[4] and chronic inflammation hypothesis[5] initialized to study AD at molecular level in the past two decades. Extra cellular deposition of Aβ is still considered as a major AD brains' pathological hallmark and the most significant target for molecular imaging.[6] Since the deposition of Aβ is found to be 10-20 years earlier than the beginning of AD symptoms,[7] noninvasive visualization of Aβ plaques such as radiopharmaceutical imaging and fluorescence imaging, have been extensively investigated.[8] Especially, quantitative positron emission tomography (PET) is still the optimal noninvasive AD diagnosis modality up to date.[9]

Grouped by their chemical backbone structures, many series of small molecular probes that can be sorted into four categories of binding sites have been synthesized and evaluated (**Figure. 1**).[8a, 10] Most of these probes derive from thioflavin-T or stilbene and share the same binding site with 6-iodo-2-(4'-dimethylamino-)phenyl-imidazo[1,2]pyridine, **1** (IMPY). All these probes were featured with a rigid conjugated planarity to fit into the hydrophobic binding channels.[11] For example, three clinical probes (2-{3-[^{18}F]Fluoro-4-(methylamino)phenyl }-1,3-benzothiazol-6-ol ([^{18}F]flutemetamol),[6, 12] (E)-4-(2-(6-(2-(2-(2-([^{18}F]-fluoroethoxy)ethoxy)ethoxy)pyridin-3-yl)vinyl)-N-methyl

benzenamine, **2** ([^{18}F]AV-45)[13] and [^{11}C]4-N-Methylamino-4´-hydroxystilbene ([^{11}C]SB-13)[14] followed this philosophy. However, these lipophilic radiotracers labeled with either ^{18}F or ^{11}C, which showed relatively high nonspecific white matter uptakes probably due to the myelin

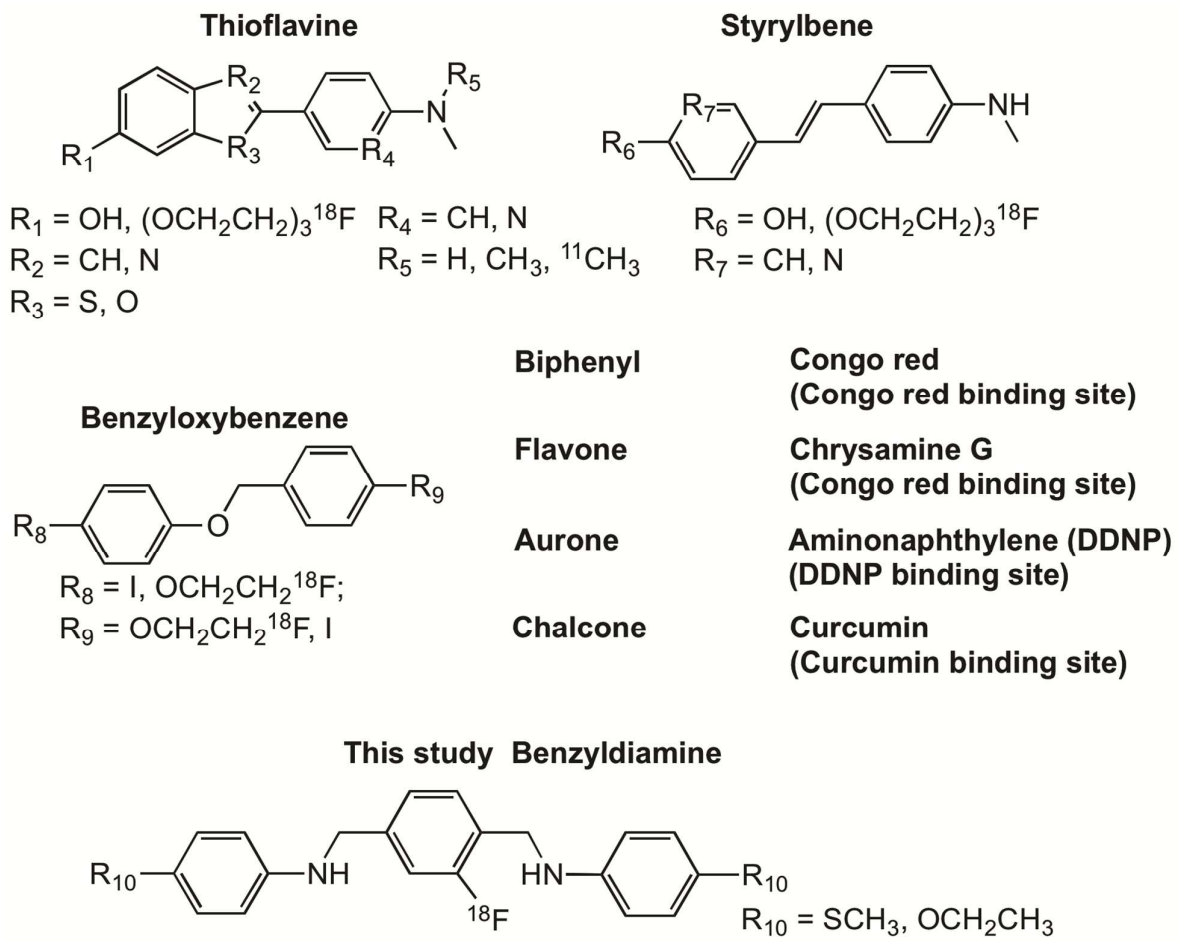

uptakes, are not capable to demarcate the borders of the gray matter where the plaque binding signals are recognized as the predominant proof of plaque deposition.[15] Thus, new PET probes with both higher affinity and selectivity for Aβ plaques still require further development.

Figure 1. Chemical structures of the previously reported PET probes of Aβ and the benzyldiamine derivatives developed in this work. The exclusive binding sites of each

category are illustrated, with not mentioned ones belonging to thioflavin T binding site.

Recently, two benzyloxybenzene derivatives (**Figure. 1**) were reported as potential A*β*-targeted agents, which are available for either ^{18}F or $^{123/125}$I labeling starting from the corresponding precursors for either single-photon emission computed tomography (SPECT) or PET.[16] Benzyloxybenzene structure is not a conjugated plane but these probes possess good affinities around 20 nM,[16a] opening new avenues of flexible compounds to improve PET imaging of AD. However, the highest affinities of these flexible benzyloxybenzene ligands rest between 10 and 100 nM, which still need to be improved for high-sensitivity PET imaging. Furthermore, their lipophilicities of current probes are too high (Log *D* = 3.62-3.96)[11] to cause potential white matter uptake problem.

Here, we described a series of flexible benzyldiamine derivatives (BDAs) and evaluated them as A*β* probes by binding affinities, binding mechanism, specificity and brain uptake profiles. A novel ^{18}F-labeling approach starting from 2-nitroterephthalaldehyde as precursor with two aldehyde groups for bi-linking were also developed. This pathway attaching ^{18}F atom on the terephthalaldehyde in the first step makes least change on BDA structure to minimize both the affinity loss by the radioactive tag and the molecular weight. The following reductive amination reaction provides lower lipophilic imine products to reduce nonspecific binding. Compared with other labeling pathways, we expect this innovation could help finding better probes for AD diagnosis and introduce more ^{18}F labeled compounds for PET.

Results and Discussion

Chemistry

BDAs (**6-13**) were synthesized following the route in **Scheme 1**. Dimethylnitroterephthalate went through hydrolysis, reduction to the dimethanol form, and further oxidized by pyridinium chlorochromate (PCC) to yield 2-nitro-terephthalaldehyde (**4**), which was the precursor as well as the intermediate for the reference compounds. Then the nitro group was replaced by fluorine through nucleophilic substitution with a yield of ~15%. The reference compounds were further obtained using one-pot reductive amination reactions using **5** for the first time with different anilines in varied yields (40-95%). Yellow Schiff bases were formed during the process as an intermediate, which were immediately reduced by $NaBH(OAc)_3$ with small amount glacial acetic acid added to accelerate the reductive process. All the crude products were further purified by silica gel chromatography, and had their structures charactered by ^{1}H NMR, ^{13}C NMR, ^{19}F NMR, and MS/HRMS.

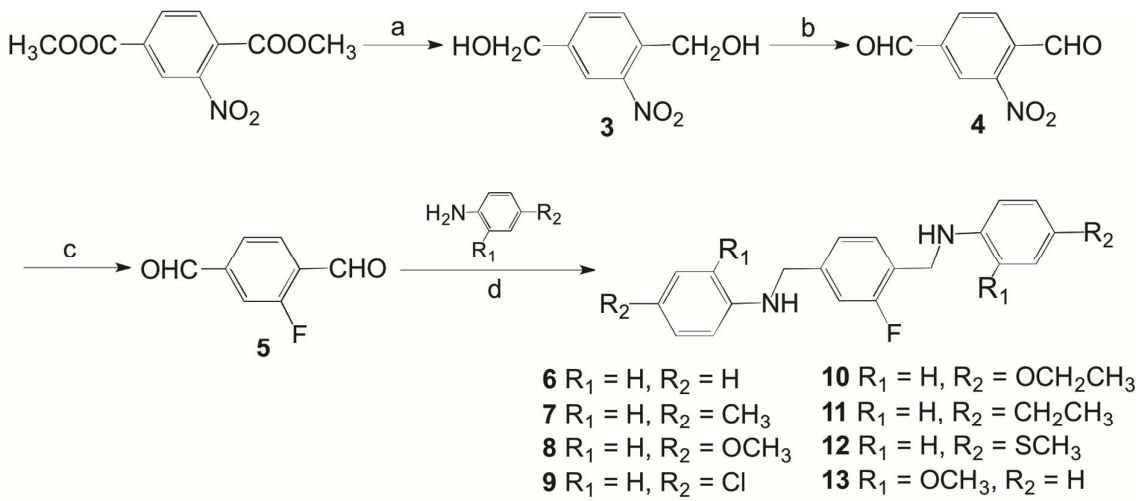

Scheme 1. Synthetic route of the precursor and reference compounds. Reagents and the conditions: a. 1) CH_3OH, NaOH, reflux, 2) $BH_3{\cdot}S(CH_3)_2$, THF, 40 °C; b. PCC, CH_2Cl_2, rt; c. 18-crown-6, KF, DMF, 140 °C; d. $NaBH(OAc)_3$, AcOH, rt.

In vitro binding studies

The quantitative affinities of BDA compounds (**6-13**) for Aβ_{1-42} aggregates were examined in the competitive binding assay. [^{125}I]**1** was used as the competing radioligand for the thioflavin T binding site[17]. **1** and **2** were screened under equal treatment as comparison, for example same concentration gradient. All tested compounds inhibited [^{125}I]**1** binding in a competitive manner dose-dependently as illustrated in **Figure 2A**. Although compounds **6-13** only differ on the substituted groups R_1 and R_2, these substituent groups dramatically affected the affinities to Aβ_{1-42} aggregates and resulted in varied K_i values from 6.8 to 2.4E3 nM. From the various affinities listed in **Figure 2B**, we can reach three conclusions. (1) The methoxyl and especially thiomethyl seem to have a favorable effect on affinity than alkyl alone. (2) When the para sites of the two symmetrical anilines are substituted by alkyl chain or alkoxy chain, The affinities would increase with the lengthening of the chain. For example, **11** (p-CH_2CH_3) has about 4-fold higher affinity than **7** (p-CH_3) while **10** (p-OCH_2CH_3) has about 3-fold higher affinity than **8** (p-OCH_3). (3) Hydrophobic substitution on ortho site instead of para site decrease affinity [K_i of **8** (p-OMe) > K_i of **13** (o-OMe)] with **13** having nearly no binding. (4) The modification on the para sites of the two symmetrical anilines with hydrophobic functional group may decrease the affinity while K_i of non-substituted **6** (p-H) exceeded 1 μM. Since the higher binding affinity is the foundation of higher sensitivity, compounds **10** (K_i = 14.9 ± 5.1 nM) and **12** (K_i = 6.8 ± 0.6 nM) were selected for ^{18}F labeling.

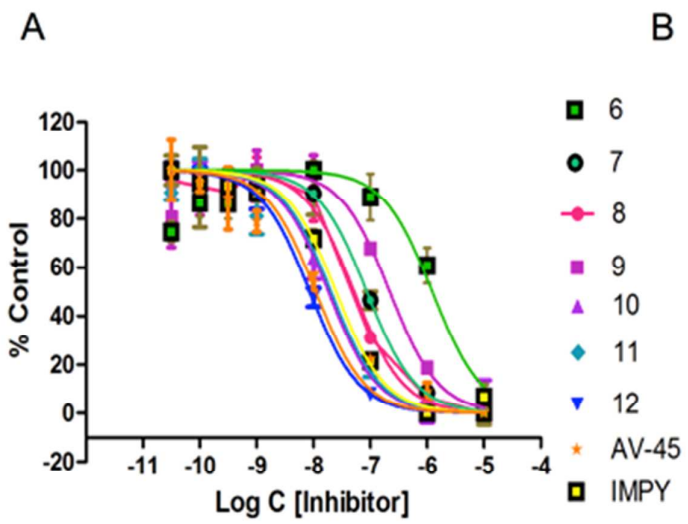

Compound	R_1	R_2	K_i[a] (nM)
6	H	H	2.14 ± 0.43 μM
7	H	CH_3	71.1 ± 3.6
8	H	OCH_3	38.5 ± 5.2
9	H	Cl	240 ± 45
10	H	OC_2H_5	14.9 ± 5.1
11	H	C_2H_5	18.5 ± 1.2
12	H	SCH_3	6.8 ± 0.6
13	OCH_3	H	>10000
AV-45			8.9 ± 1.5
IMPY			19.8 ± 1.6

[a] n = 3

Figure 2. (A) Inhibition curves of [^{125}I]1 binding to A$\beta_{1–42}$ aggregates by **1**, **2**, **6-13**. (B) Inhibition constants (K_i, nM) of BDAs. Results are given as the mean ± SD, n = 3.

Molecular docking

Molecular docking technique[18] was applied to explore the underlying mechanism of these newly proposed Aβ agents. First of all, geometry optimization of compound **10** and **12** in water phase was executed at the B3LYP/6–31G level.[19] As illustrated in **Figure 3A**, the optimized geometry of compound **12** was a stair-shape flake with the dihedral angles about 92 degree between each aniline plane and the benzyl plane. Although this most favorable geometry seems twisted, those sigma bonds are dynamically rotating that the molecule keeps transforming between a flatter stair and a steep one. Then the binding to A$\beta_{1\text{-}42}$ fibril model with two-fold symmetry (PDB ID: 2LMO)[20] was investigated by molecular docking. The result indicated that the similar binding pocket with **1** was revealed (**Figure 3B-E**). We speculate that when compound **12** rotates itself into a mildly twisted or near flat geometry

(dihedral angles between each aniline plane and the benzyl plane <31 degree), it will snuggle into the channels on the side-chain ladders formed by hydrophobic Val18_Phe20. Distinguished from other rigid molecule cases, the binding of **12** could happen whenever the dihedral angle is sharper than 31 degree, which may assign a higher probability. The binding affinity is a measurement of the attraction strength between a receptor and its ligand, and could be represented by the binding energy mostly determined by the strength of hydrogen bonding, Van der Waals forces and hydrophobic bonds. The lowest calculated binding energy for **12** is -6.8 kcal/mol, more negative compared to -4.95 kcal/mol for **1** to A$\beta_{1\text{-}42}$,[16a] suggesting **12** dose fit tightly into the binding pocket with lower binding energy and potential higher affinity.

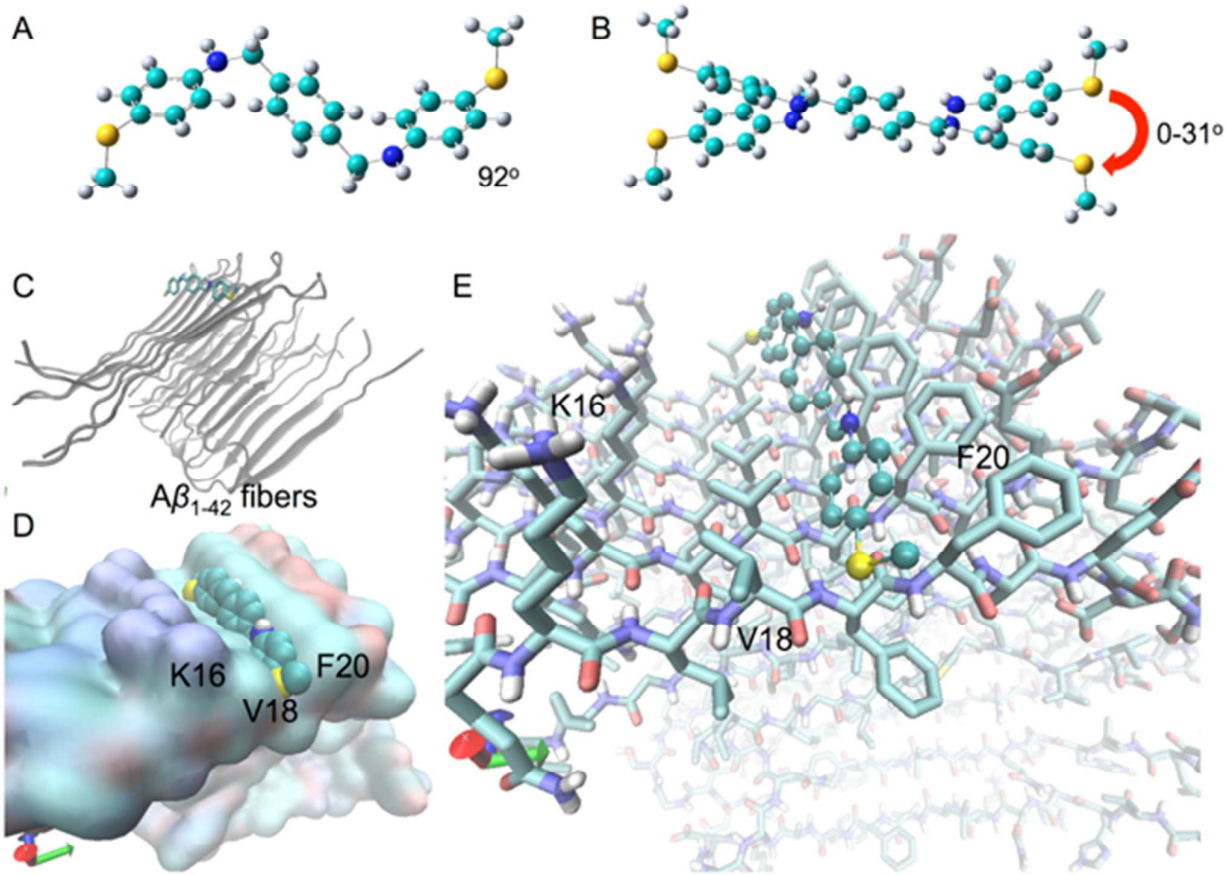

Figure 3. Computational studies. (A) Geometry optimization of compound **12** in water phase. (B) Geometry variation of "able-to-bind" compound **12**, of which the dihedral angles between each aniline plane and the benzyl plane <31 degree. (C) An overview of **12** and A$\beta_{1\text{-}42}$ fiber. (D, E) Molecular docking results indicated that the near-flat geometric configuration of **12** bound to the channels formed on side-chain ladders by hydrophobic Val18_Phe20, resembling the computational binding behavior of **1**.[21]

Radiolabeling

Following the scheme in **Figure 4A**, the ^{18}F labeled intermediate 2-fluoroterephthalaldehyde ([^{18}F]**5**) was prepared at 140 °C within 10 min at an average radiochemical yield 74 ± 5% (n = 5, decay corrected) after purification by a Sep-Pak plus C18 cartridge (Waters, USA). 5-10 min heating for the nucleophilic substitution of nitro group was proper due to that the aldehyde on the benzene might be oxidized overtime by DMSO. Then [^{18}F]**5** was eluted with 1.0 mL 1,2-dichloroethane and went through a reductive amination reaction with corresponding anilines to yield [^{18}F]**10** and [^{18}F]**12**, respectively. Glacial acetic acid was added to accelerate the reduction process to about 15 min. Radiochemical yields in this step were 51 ± 6% (n = 5, decay corrected), giving an average total yield of 35 ± 6% (n = 5, decay corrected, at synthesis end). Radiochemical purity after semi-preparation high performance liquid chromatography (HPLC) purification was more than 95%. The identities of [^{18}F]**10** and [^{18}F]**12** were performed by co-injection of the nonradioactive standard compounds (**Figure 4B**), with time differences that depends on dead volumes between detectors (~ 1.0 min). Specific activities were calculated to be 49 ± 8 GBq/μmol (n = 5, at the end of synthesis), comparable with other ^{18}F labeled probes for plaques.

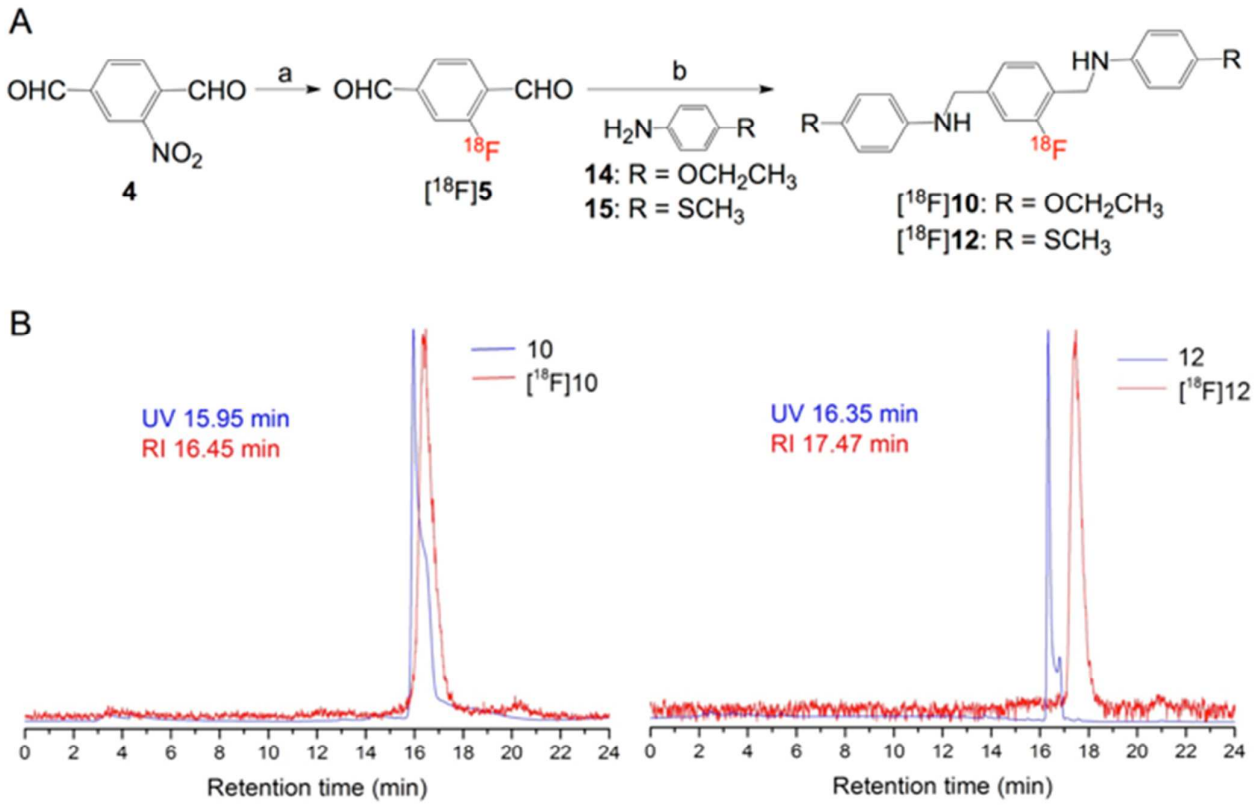

Figure 4. Radiosynthesis. (A) Radiosynthetic route. Reagents and conditions: a. $K^{18}F$, K_{222}, DMSO, 140 °C, 5-10 min; b. $NaBH(OAc)_3$, AcOH, rt, 15 min. (B) HPLC profile of co-injection of **10** and [^{18}F]**10**, **12** and [^{18}F]**12**. Analytical HPLC conditions: gradient elution (0-5 min, 40% B, 5-10 min, 40-80% B, 10-20 min, 80% B, 20-30 min, 80-40% B. Eluent A was phosphate buffer, pH = 7.4, and eluent B was CH_3CN.) was performed by an analytical C18 column (Venusil MP C18, Agela Technologies, 5 μm, 4.6 × 250 mm). UV detector, 254 nm.

Octanol-water partition coefficients

The lipo-hydro partition coefficients (Log *P*) of [^{18}F]**10** and [^{18}F]**12** were measured in a 1-octanol/PBS (pH = 7.4) system respectively to estimate their blood brain barrier (BBB)

penetrating abilities. 1.12 ± 0.09 for [^{18}F]**10** and 0.94 ± 0.21 for [^{18}F]**12** fall in our ideal range which is more hydrophilic than traditional Aβ probes (Log P = 2-3) to allow both sufficient penetration of BBB and reduced non-specific binding.[22]

Biodistribution

After i.v. injection of [^{18}F]**10** or [^{18}F]**12** in saline containing 2.5-5% ethanol (v/v) to ICR (Institute of cancer research) mice, uptakes of radioactivity in organs of interest were measured and showed in **Figure 5**. With similar lipophilicity, molecular weights and structures, the initial uptakes of [^{18}F]**10** and [^{18}F]**12** at 2 min were 2.10 ± 0.37 %ID/g and 4.87 ± 0.52 %ID/g, respectively. Initial brain uptake of [^{18}F]**12** is higher compared with [^{18}F]**10** and is more suitable as a brain imaging probe (**Table 1**).The $brain_{2min}/brain_{60min}$ ratios were 5.38 for [^{18}F]**10**, and 4.38 for [^{18}F]**12**, indicating similar clearance speed acceptable for cerebral PET imaging. Bone uptakes of both tracers decreased from 2 to 60 min showing that there was no significant defluorination *in vivo*. However, other metabolic natures between [^{18}F]**10** and [^{18}F]**12** are distinct from each other. The blood and kidney uptakes of [^{18}F]**10** were low and decreasing slowly over time. The lung and liver uptakes both summited at 10 min and remained remarkable until 60 min post-injection. We speculate that hydrophobic aggregation of [^{18}F]**10** might have happened in lung. Elimination was mostly in liver and partially in stomach and intestinal for [^{18}F]**10**, because remarkable accumulation of radioactivity were also detected. In contrast, [^{18}F]**12** exhibited no significant concentration in the liver and stomach, but a quite notable uptake at kidney at 2 min followed by rapid elimination and continuous intense intestine uptake greater than 4 %ID/g.

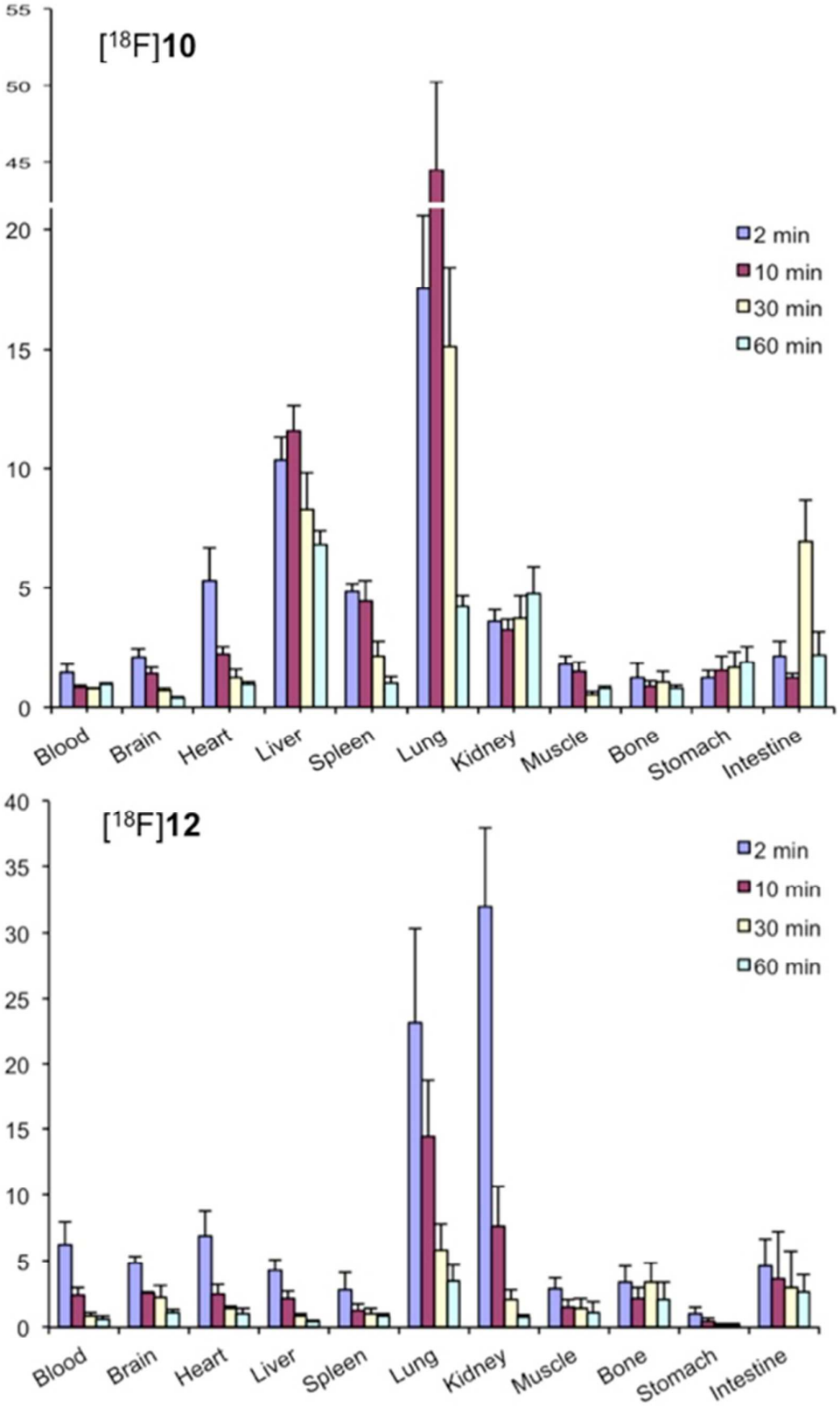

Figure 5. Biodistribution histogram of [^{18}F]**10** and [^{18}F]**12** in male ICR mice. Expressed as averages for 5 mice ± standard deviation in % injected dose per gram (%ID/g).

Table 1. Brain and blood uptakes of [^{18}F]**10** and [^{18}F]**12** in male ICR mice[a].

Probe	Selected tissue	2 min	10 min	30 min	60 min
[^{18}F]**10**	Blood	1.46 ± 0.33	0.81 ± 0.09	0.76 ± 0.03	0.97 ± 0.04
[^{18}F]**10**	**Brain**	**2.10 ± 0.37**	**1.38 ± 0.27**	**0.68 ± 0.08**	**0.39 ± 0.04**
[^{18}F]**12**	Blood	6.22 ± 1.74	2.44 ± 0.58	0.87 ± 0.21	0.59 ± 0.30
[^{18}F]**12**	**Brain**	**4.87 ± 0.52**	**2.58 ± 0.10**	**2.25 ± 0.86**	**1.11 ± 0.24**

[a] Expressed as %ID/g, n = 5.

In vitro and in vivo stabilities of [^{18}F]12

After incubating for 60 min in saline or mouse plasma at 37 °C, much more than 95% radioactivity was identified by HPLC as intact compound [^{18}F]**12** (**Figure S25 A, B**). More importantly as an *in vivo* imaging agent for brain, metabolism of [^{18}F]**12** in blood and brain of normal ICR mice was further evaluated by HPLC analysis obtained 60 min post-injection (**Figure S25 C, D**). [^{18}F]**12** displayed moderate stability in the blood and brain, with 75.9 ± 3.5 % and 62.1 ± 5.3 % of the original probe after 60 min, respectively.

5×FAD mice model

Aβ plaques, gliosis, synaptic markers reduction, and neuron loss have been reported on this five time FAD (5×FAD) transgenic mice model with a total of five familial Alzheimer's disease (FAD) mutations co-expressed.[23] These mice were supposed to produce cerebral Aβ plaques as early as two months old and become severer when older.[24] Immunofluorescence staining with mouse anti-Aβ monoclonal antibody 6E10 (Covance Antibody, 1:20000) was

conducted to confirm its existence in the cortex on 5-11 months models. Compared with the wild type mouse cortex, typical Aβ plaques with diffused boundary were clearly stained (**Figure 6**).

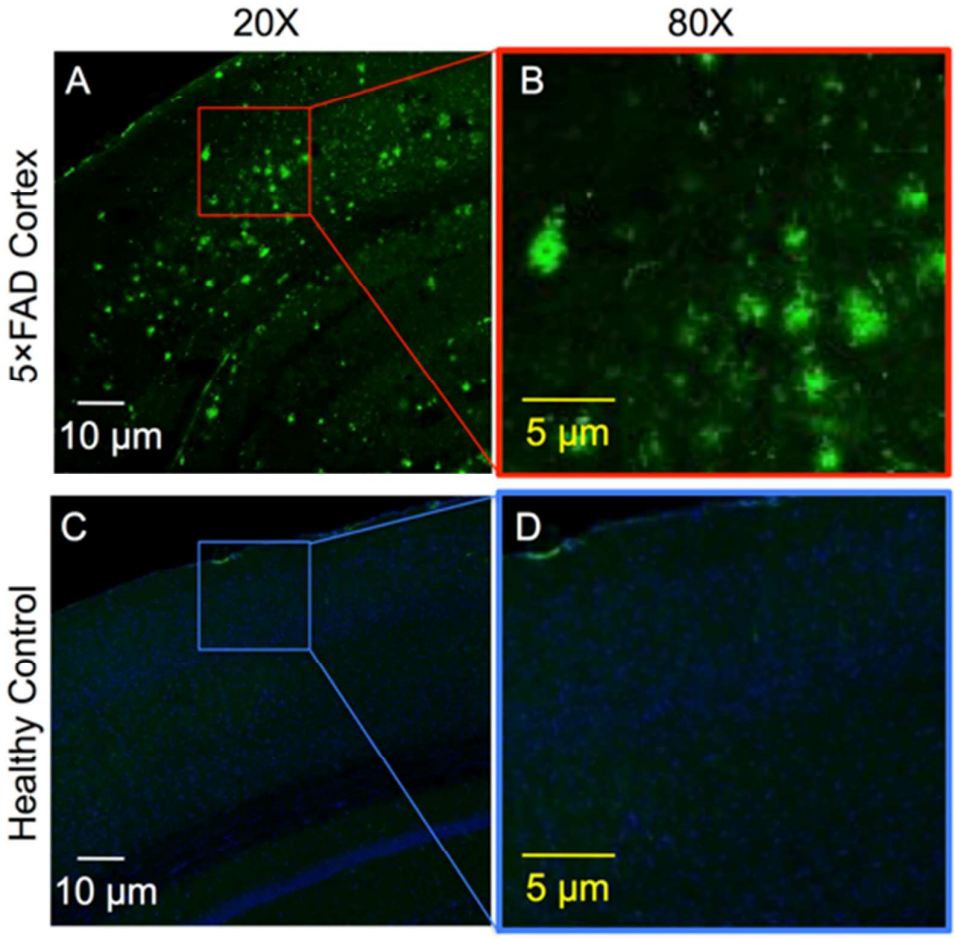

Figure 6. Immunofluorescence staining of Aβ on a brain section of a 5×FAD mouse (male,7 month) with 6E10 antibody. (A, B) Photomicrographs in the cortex field. (C, D) Healthy control.

MicroPET-CT imaging

5×FAD mice (male, 5-7 month old) and same age male wild-type mice (control) were employed in microPET-CT imaging (n = 3) with [^{18}F]**12**, [^{18}F]**2** and [^{18}F]FDG.

Anesthetization was conducted with 2.5% isoflurane during preparation and 1.5% during scans. 5 min static whole-body microPET scans were acquired by an Siemens Inveon microPET-CT (Siemens, Germany) 30 min after intravenous injection of [^{18}F]**12** (100 μL, 1.85 ± 0.50 MBq), [^{18}F]**2** (100 μL, 1.85 ± 0.50 MBq), [^{18}F]FDG (100 μL, 3.7 ± 0.5 MBq), respectively. Reconstruction of PET images was performed with three-dimensional ordered subset expectation maximization (2D OSEM) algorithm. For comparison, regions of interest (ROIs) were drawn on the brain, cerebellum, bone etc. according to the CT templates and then added to the co-registered PET images. MicroPET-CT images implied that [^{18}F]**12** can differentiate AD and normal brain 30 min post injection, and able to be washed out from the normal brain regions quickly (**Figure. 7A, B**). The imaging result are similar compared with the images by [^{18}F]**2** (**Figure. 7C, D**) but white matter uptake were lower by [^{18}F]**12** as the white arrows marked in **Figure. 7A**, with low uptake areas and median fissure more clearly illustrated. The cerebral uptakes of [^{18}F]FDG showed that less radioactivity detained in the brain of model brains than control, which indicated weak brain functions to assist the AD brain diagnosis **(Figure 7E, F**). No notable bone and muscle uptakes were found during the sustained scans.

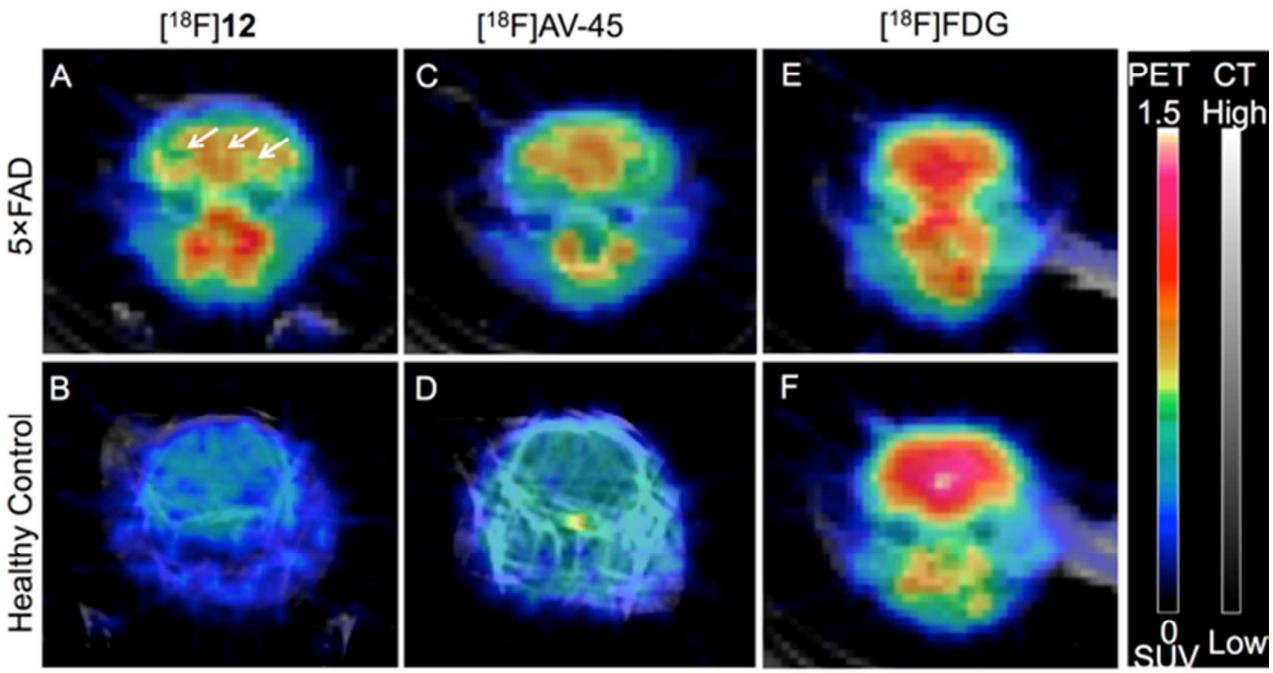

Figure 7. MicroPET-CT imaging of brain. (A, B) Transversal brain PET images of [^{18}F]**12** superimposed onto CT templates. (C, D) [^{18}F]**2**. (E, F) [^{18}F]FDG.

Standardized uptake values (SUV) of respective probes were measured and calculated for the cerebral and listed in **Table 2**. The 5×FAD mice cerebral SUV of [^{18}F]**12** was 3.46 ± 0.33, slightly lower than [^{18}F]**2**. However, since its control mice cerebral SUV was even lower, the cerebral SUV ratio$_{5\times FAD/control}$ of [^{18}F]**12** was slightly superior than [^{18}F]**2**.

Table 2. Cerebral SUVs from PET images.

Probe	[^{18}F]**12**	[^{18}F]**2**	[^{18}F]FDG
5×FAD cerebral	3.46 ± 0.33[a]	3.68 ± 0.46	5.46 ± 0.53
Control cerebral	1.03 ± 0.37	1.35 ± 0.27	6.78 ± 0.28

$Ratio_{5\times FAD/control}$	3.35	2.72	0.80

[a] SUV-bw = average activity in ROI (Bql/mL) / injected dose (Bql) × subject weight (g), n = 3.

Conclusions

A series of fluorinated BDA derivatives beyond the traditional field of effective structures were designed, synthesized and screened for PET targeting cerebral A*β* plaques. The aromatic rings of the BDA compounds were connected with flexible sigma bonds and unable to form a plenary π-conjugated system. Taking advantage of the good tolerance of A*β*, BDA compounds competed well against **1** with different binding affinities to $A\beta_{1\text{-}42}$ aggregates. The K_i values differ from 6.8 ± 0.6 nM, best ever of this kind as a flexible probe, to ~2E3 nM. Molecular docking predicted excellent binding to A*β* fibers. Consequently, [^{18}F]**10** and [^{18}F]**12** with favorable binding affinities (K_i = 14.9 ± 5.1, and 6.8 ± 0.6 nM, respectively) were reproducibly synthesized in radiochemical yields greater than 30%. In biodistribution study, the ^{18}F-labeled ligands displayed satisfactory *in vivo* uptake profile. Especially, [^{18}F]**12** exhibited high brain uptake with 4.87 %ID/g 2 min post-injection, moderate clearance with $brain_{2\ min}/brain_{60\ min}$ ratio of 4.38, but no significant deflouronation. Meanwhile, [^{18}F]**12** displayed acceptable biostability in mouse blood and plasma (intact form > 95% at 60 min). Decomposition of [^{18}F]**12** in the brain can't be ignored (intact form about 62% at 60 min), which should be improved in the following studies for A*β* imaging. MicroPET-CT images implied that all [^{18}F]**12** can penetrate the BBB to target and produce enough signals for detection which is comparable with the images of [^{18}F]**2**. The $ratios_{AD/control}$ of [^{18}F]**12** and

[^{18}F]**2** during proper imaging window are better than the reported ratio$_{AD/control}$ of [^{11}C]Pittsburgh compound-B in human.[25] Since the imaging data on AD model mice by the ^{18}F labeled benzyloxy derivatives has not been reported, comparison of imaging abilities between flexible probes has not been available yet. In conclusion, Aβ fiber binding pocket exhibited good tolerance to BDA ligands distortion. And this innovative finding favors the new standpoint that the planar rigid molecular with π-conjugated system was dispensable, providing new hints for developing targeting ligands with flexible framework for improving localization and quantitative PET imaging.

Experimental

General information

Reagents used in the synthesis were purchased from J&K Scientific Ltd. (China) and applied without further purification. The reactions were monitored with Thin Layer Chromatography on Silica gel 60 F254 aluminum sheets (Merck, Germany), where compounds were visualized with a 254 nm UV lamp. Column chromatography purifications were conducted on 54 - 74 μm silica gel (Qingdao Haiyang Chemical, China). The melting points of newly synthesized compounds are detected by a MPA100 automated melting point system (OptiMelt, USA). ^{1}H NMR, ^{13}C NMR and ^{19}F NMR characterization of our synthesized compounds dissolved in $CDCl_3$ was performed on a 400 MHz Spectrometer (Avance II, Bruker, Germany) with tetramethylsilane as an internal standard. Mass spectra were acquired with the amazon SL Bruker instrument or the Bruker Equire 3000 plus (ESI) instrument. HPLC analysis and purification were performed on a Thermo Scientific Dionex Ultimate

3000 system equipped with SPD-20A UV detector (λ = 254 nm) as well as a Bioscan Flow Count 3200 NaI/PMT γ-radiation detector. Thermo Scientific Hypersil Gold columns (250×4.6 mm, 250×10 mm) were employed at a flow rate of about 1.0 mL/min for analysis and 4.0 mL/min for separation. Mobile phase A, phosphate buffer, pH = 7.4. Phase B, HPLC grade acetonitrile (Amethyst Chemicals, China). The elution sequence was 40% B (0-5 min), 40-80% B (5-10 min), 80% B (10-20 min), 80-40% B (20-25 min). Radioactivity was measured on a WIZARD^2 2480 automatic gamma counter (PerkinElmer, USA). The centrifuge we used in Log *D* determination was Eppendorf Centrifuge 5424 R (Germany). All mice protocols were approved by Xiamen University Animal Care Association. [^{18}F]Fluoride and [^{18}F]FDG was obtained from the First Affiliated Hospital of Xiamen University.

(2-Nitro-1,4-phenylene)dimethanol (3)

5.0 g dimethylnitroterephthalate was dissolved in 80 mL methanol. 22 mL NaOH (2.0 M) solution was added to the mixed solution which was afterwards heated to 60 °C for 5 h before cooling down to the room temperature. Then the reaction mixture was quenched with HCl (2.0 M) and concentrated under vacuum. The precipitation was filtered and dried to obtain 4.3 g product at a yield of 98%. 2.0 g (9.5 mmol) of the solid product was gently dissolved in 50 mL THF in a 100 mL double neck bottle. A solution of borane-methyl sulfide complex in THF (2.0 M, 25 mL, 50 mmol) was added dropwise at 0 °C under nitrogen. Then the reaction mixture was stirred for 18 h at 40 °C before quenching with 20 mL NaOH aqueous solution (1.0 M). THF was removed in vacuum and the remaining aqueous solution was extracted with ethyl acetate (2 × 50 mL). After the organic layers was combined and dried with

anhydrous sodium sulfate, it was evaporated under reduced pressure to obtain pure pale-yellow solid (1.6 g, 92%). ^{1}H NMR (400 MHz, $CDCl_3$) δ 4.58 (d, 2H, J = 5.82 Hz); 4.79 (d, 2H, 5.28Hz); 5.46 (t, 1H, J = 5.71 Hz); 5.50 (t, 1H, J = 5.58 Hz); 7.68 (d, 1H, J = 8.29 Hz); 7.67 (d, 1H, J = 8.03 Hz); 7.97 (s, 1H).

2-Nitroterephthalaldehyde (4)

PCC (6.5 g, 30.4 mmol) was added into a solution of **3** (1.4 g, 7.6 mmol) in 200 mL CH_2Cl_2 while stirring. The reaction mixture was kept stirred at room temperature for 5 h before a second portion of PCC (1.6 g, 7.6 mmol) was added and kept stirred further for 2 h. We concentrated the reaction mixture to 50 mL under vacuum, and loaded it onto a silica gel column, which was eluted with CH_2Cl_2, fractions containing the product was collected (TLC: ethyl acetate/petroleum ether 1:2, Rf 0.5) and evaporated under vacuum to yield a pale-yellow solid product (0.8 g, 58%). ^{1}H NMR (400 MHz, $CDCl_3$): δ 8.07 (d,1H, J = 7.74 Hz); 8.37 (dd, 1H, J_1 = 7.87 Hz, J_2 = 1.02 Hz); 8.61 (d, 1H, J = 1.43 Hz); 10.17 (s, 1H); 10.31 (s, 1H).

2-Fluoroterephthalaldehyde (5)

Anhydrous potassium fluoride (64 mg, 1.1 mmol), 18-crown-6 (300 mg, 1.1 mmol) were dissolved in 1.0 mL anhydrous DMF in a 10 mL serum vial (WHEATON, USA). After 5 min stirring at room temperature, **4** (100 mg, 0.65 mmol) dissolved in 0.2 mL anhydrous DMF was added into the vial. This mixture was placed into 140 °C oil bath for 7 min. After quenching by 5 mL water, the mixture was extracted with ethyl acetate (2 × 5 mL). Organic

layers were collected and dried. Evaporated under vacuum, the resulting residue was purified by column chromatography on silica gel to yield **5** (12 mg, 14%). TLC rf 0.4 (ethyl acetate/petroleum ether 1:4). ^{1}H NMR (400 MHz, $CDCl_3$): δ 7.71 (d, 1H, *J* = 9.90 Hz); 7.81 (d, 1H, *J* = 7.75 Hz); 8.07 (t, 1H, *J* = 6.73 Hz); 10.09 (d, 1H, *J* = 1.76 Hz); 10.46(s, 1H). ^{19}F NMR (376 MHz, $CDCl_3$): δ -119.37 (s, 1F).

General procedure for the reductive amination reaction (A).

A mixture of 2-fluoro-1,4-benzenedialdehyde (1 equivalent), aniline (2 equivalent) and sodium triacetoxyborohyride (2 equivalent) in 1,2-dichloroethane was stirred for 10 min before AcOH (1 equivalent) was added. 3 h later, 1.0 M NaOH (1 mL) was added to quench the reaction. The solution was drawn with ethyl acetate (3 × 3 mL). The organic phase was collected, dried and concentrated under reduced pressure to produce a pale yellow oil residue. The crude product was purified through column chromatography to yield a white solid product.

N,N'-((2-Fluoro-1,4-phenylene)bis(methylene))dianiline (6)

This compound was prepared in the same way detailed in general procedure A as a white solid (44.1%, m.p. 105 ± 2 °C). TLC Rf = 0.5 (ethyl acetate/petroleum ether 1:6). ^{1}H NMR (400 MHz, $CDCl_3$) δ 4.33 (s, 2H); 4.38 (s, 2H); 4.37 (s, 2H); 6.64 (dd, 4H, J_1 = 13.81 Hz, J_2 = 7.69 Hz); 6.74 (t, 2H, *J* = 7.33 Hz); 7.11 (m, 2H); 7.19 (m, 4H); 7.35 (t, 1H, 7.70 Hz). ^{19}F NMR (376 MHz, $CDCl_3$) δ -118.76 (s, 1F). ^{13}C NMR ($CDCl_3$, 100 MHz): δ 114.9, 115.9, 116.2, 121.6, 124.9, 125.5, 130.1, 130.5, 141.0, 144.1, 149.2, 162.6, 165.1, 188.7. HRMS

calcd for $C_{20}H_{20}FN_2^+$, 307.1606, found 307.1608 $[M + H]^+$.

***N,N'-((2-Fluoro-1,4-phenylene)bis(methylene))bis(4-methylaniline)* (7)**

This compound was obtained in the same way detailed in general procedure A as white solid (55%, m.p. 112 ± 1 °C). ^{1}H NMR (400 MHz, $CDCl_3$) δ 2.24 (s, 6H); 4.30 (s, 2H); 4.36 (s, 2H); 6.56 (dd, 4H, J_1 = 14.52 Hz, J_2 = 8.20 Hz); 6.99 (d, 4H, J = 7.68 Hz); 7.08 (d, 2H, J = 10.45 Hz); 7.33 (t, 1H, J = 7.76 Hz). ^{19}F NMR (376 MHz, $CDCl_3$) δ -118.76 (s, 1F). HRMS calcd for $C_{22}H_{24}FN_2^+$, 335.2, found 334.9 $[M + H]^+$.

N,N'-((2-Fluoro-1,4-phenylene)bis(methylene))bis(4-methoxyaniline) (8)

This compound was obtained in the same way detailed in general procedure A as a pale yellow solid (95%, m.p. 116 ± 1 °C). ^{1}H NMR (400 MHz, $CDCl_3$) δ 3.73 (s, 6H); 4.26 (s, 2H); 4.32 (s, 2H); 6.59 (dd, 4H, J_1 = 23.69 Hz, J_2 = 8.80 Hz); 6.76 (d, 4H, J = 6.89 Hz); 7.08 (m, 2H); 7.32 (t, 1H, J = 7.56 Hz). ^{13}C NMR ($CDCl_3$, 100 MHz): δ 42.6, 48.5, 55.8, 114.3, 114.9, 129.7.5, 141.4, 142.0, 152.4, 160.3. ^{19}F NMR (376 MHz, $CDCl_3$) δ -118.76 (s, 1F). HRMS calcd for $C_{22}H_{24}FN_2O_2^+$, 367.1817, found 367.1808 $[M + H]^+$.

N,N'-((2-Fluoro-1,4-phenylene)bis(methylene))bis(4-chloroaniline) (9)

This compound was obtained in the same way detailed in general procedure A as a pale yellow solid (40%, m.p. 109 ± 1 °C). ^{1}H NMR (400 MHz, $CDCl_3$) δ 4.29 (s, 2H); 4.34 (s, 2H); 6.53 (dd, 4H, J_1 = 21.36 Hz, J_2 = 8.62 Hz); 7.05-7.12 (m, 6H); 7.29 (t, 1H, 7.59 Hz). ^{19}F NMR (376 MHz, $CDCl_3$) δ -118.76 (s, 1F). HRMS calcd for $C_{22}H_{18}Cl_2FN_2^+$, 375.0826, found

375.0819 $[M + H]^+$.

N,N'-((2-Fluoro-1,4-phenylene)bis(methylene))bis(4-ethoxyaniline) (10)

Similar to above, this compound was prepared in the same way detailed in general procedure A as pale yellow solid (45%, m.p. 119 ± 1 °C). ^{1}H NMR (400 MHz, $CDCl_3$) δ 1.38 (t, 6H, J = 6.98 Hz); 3.96 (q, 4H, J = 6.95); 4.27 (s, 2H); 4.33 (s, 2H); 6.59 (dd, 4H, J_1 = 15.48 Hz, J_2 = 8.75 Hz); 6.78 (d, 4H, J = 8.90 Hz); 7.08 (d, 1H, J = 3.59 Hz); 7.11 (s, 1H); 7.34 (t, 1H, J = 7.54 Hz); ^{19}F NMR (376 MHz, $CDCl_3$) δ -118.76 (s, 1F). HRMS calcd for $C_{22}H_{28}FN_2O_2^+$, 395.2130, found 395.2123 $[M + H]^+$.

N,N'-((2-Fluoro-1,4-phenylene)bis(methylene))bis(4-ethylaniline) (11)

Similar to above, this compound was obtained as a white solid (43%, m.p. 119 ± 1 °C). ^{1}H NMR (400 MHz, $CDCl_3$) δ 1.20 (t, 6H, J = 7.57Hz); 2.56 (q, 4H, 7.54 Hz); 4.31 (s, 2H); 4.37 (s, 2H); 6.59 (dd, 4H, J_1 = 14.24 Hz, J_2 = 8.05 Hz); 7.02 (d, 4H, J = 7.92 Hz); 7.08 (d, 1H, J = 3.59 Hz); 7.12 (s, 1H); 7.35 (t, 1H, J = 7.52 Hz). ^{13}C NMR ($CDCl_3$, 100 MHz): δ 15.9, 27.9, 42.0, 47.9, 113.0, 114.2, 122.9, 128.6, 129.7, 133.7, 144.3, 145.8, 160.3. ^{19}F NMR (376 MHz, $CDCl_3$) δ -118.76 (s, 1F). MS calcd for $C_{22}H_{28}FN_2^+$, 363.2, found 362.8 $[M + H]^+$.

N,N'-((2-Fluoro-1,4-phenylene)bis(methylene))bis(4-(methylthio)aniline) (12)

This compound was obtained in the same way detailed in general procedure A s a red-brown solid (69%, m.p. 121 ± 1 °C). ^{1}H NMR (400 MHz, $CDCl_3$) δ 2.41 (s, 6H); 4.32 (s, 2H); 4.37 (s, 2H); 6.58 (dd, 4H, J_1 = 13.96 Hz, J_2 = 8.59 Hz); 7.08 (d, 1H, J = 5.40 Hz); 7.10 (s, 1H);

7.21 (d, 4H, J = 8.12 Hz); 7.31 (t, 1H, J = 8.10 Hz). ^{19}F NMR (376 MHz, $CDCl_3$) δ -118.76 (s, 1F). HRMS calcd for $C_{22}H_{24}FN_2S_2^+$, 399.1360, found, 399.1353 $[M + H]^+$.

N,N'-((2-(Fluoro-18F)-1,4-phenylene)bis(methylene))bis(2-methoxyaniline) (13)

Similar to the above, this compound was prepared in the same way detailed in general procedure A as a pale-yellow solid (48%, m.p. 116 ± 1 °C). ^{1}H NMR (400 MHz, $CDCl_3$) δ 1.55 (s, 6H); 4.29 (s, 2H); 4.34 (s, 2H); 6.53 (dd, 4H, J_1 = 21.52 Hz, J_2 = 8.71 Hz). ^{13}C NMR ($CDCl_3$, 100 MHz): δ 41.3, 47.3, 55.4, 109.5, 110.1, 114.1, 116.9, 121.3, 122.9, 125.1, 129.6, 137.8, 141.2, 146.9, 160.3. ^{19}F NMR (400 MHz, $CDCl_3$) δ -118.76 (s, 1F). HRMS calcd for $C_{22}H_{24}FN_2O_2^+$, 367.1817, found, 367.1809 $[M + H]^+$.

In vitro binding assay

In vitro binding assay was conducted in the same way detailed in a previous literature.[26]

Molecular docking

Compound **12** was constructed with GaussView 5.0 (Gaussian, Inc., USA) firstly. Geometric optimizations were performed in the water phase in Gaussian 09 Revision C.01 (Gaussian, Inc., USA) using B3LYP/6-31G[19] for all atoms. Docking simulations on Aβ fibers (PDB ID: 2LMO[20]) performed according to previously described methods.[16a] For the docking simulations, the C-N bonds were kept flexible. The grid size was chosen to occupy the whole ligand-peptide complex, and the spacing was kept to 1.00 Å, a standard value for Autodock Vina[27]. Each docking trial produced 100 poses with the exhaustiveness value of 100.

Radiolabeling

The ^{18}F radiolabeled intermediate [^{18}F]**5** was prepared according to the following procedure. $^{18}F^-$ was trapped, eluted and dried following a routine procedure described in a previous literature.[26] 5.0 mg Nitro terephthalaldehyde dissolved in 0.5 mL anhydrous dimethyl sulphoxide (DMSO) was added into the serum vial containing the K_{222}-$^{18}F^-$ complex and kept heating at 140 °C. After 5 min reaction, the vial was taken out from the oil bath, cooled down to ambient temperature by running tap water. 8 mL water was added into the mixture, before this DMSO/water solution was passed through a Sep-Pak plus C18 cartridge (waters, USA). Washed with additional 5 mL water, and the desired intermediate [^{18}F]**5** was eluted by ~1.0 mL of 1,2-dichloroethane into a new serum vial. The appropriate amines (**14** or **15**, 2 mg) and $NaBH(OAc)_3$ (5 mg) were added into the eluted solution. Stirred for 2 min at room temperature, glacial acetate acid (4 μL) was injected in to promote the reductive amination process. We stirred the mixture at room temperature for another10 min. NaOH aqueous (1.0 M, 100 μL) was added to quench the reaction. Then the radiolabeled product was exacted with ethyl acetate (1 mL), and dried over $NaSO_4$. The organic solvent was evaporated under nitrogen gas and the residue was dissolved in HPLC eluent for separation. After HPLC purification, the radiochemical purity of [^{18}F]**10** and [^{18}F]**12** was bigger than 95%. The retention time of [^{18}F]**10** and [^{18}F]**12** were 16.45 and 17.47 min, respectively. For formulation, the fluid collected from HPLC (HPLC mobile phase during product collection was 80% acetonitrile and 20% water) was dried with N_2 flow and further dissolved in saline mixed with 2.5% ([^{18}F]**10**) or 5% ([^{18}F]**12**) ethanol (v/v) to make the final concentration to be 18.5

MBq/mL. Purity and specific activity were sent to analytical HPLC before experiments *in vitro* or *in vivo*. 0.1 mL of this probe solution was injected into each model mice to deliver 1.85 MBq for both biodistribution and imaging experiments. Our injected doses were all lower than 2.0 MBq with specific activity determined to be 49 ± 8 GBq/μmol (n = 5, at the end of synthesis) in saline containing no more than 5% (v/v) ethanol, which met the requirement of safety for animal in this proof-of-concept study.

Partition Coefficient Determination

Partition coefficients (Log *P*) of [^{18}F]**10** and [^{18}F]**12** were measured in 1-octanol and phosphate buffered saline (PBS), which were pre-equilibrated with each other. About 10 μCi of [^{18}F]**10**/**12** in water (0.1 mL) after HPLC purification was added in a plastic centrifuge tube (GEB, Hangzhou Gene Era Biotech Co., Ltd., China), to which 1.9 mL of PBS and 2 mL octanol was added followed. The tube was vortexed for 5 min followed by 5 min of centrifugation. Aliquots of 0.1 mL from each phase were measured in an automatic gamma counter. Partition coefficient was expressed as *Log P*. *P* (equals to *D* in this study) was calculated as the formula: *D* = (Counts in 1-octanol/Counts in PBS). The measurement was performed in triplicate.

In vitro and in vivo stability studies

After incubation or *in vivo* biodistribution of [^{18}F]**12**, the plasma (the mice were sacrificed by decapitation for blood collection) or ultrasonicated organ samples were precipitated by adding 100 μL acetonitrile and centrifuged at 3000 rpm for 5 min. 10 μL supernatants were

analyzed by HPLC respectively.

Immunofluorescence study

In vitro binding assay was conducted in the same way detailed in a previous literature.[24]

Biodistribution

Twenty ICR mice (male, 18-20 g, 5-6 weeks old) were allowed water and food ad libitum, and randomly selected for each group by removing from their cages without selection. The injected doses were measured by a CRC-25R dose calibrator (CAPINTEC, USA) with the syringe residue activities deducted. 1.85 ± 0.50 MBq of [^{18}F]**10** or [^{18}F]**12** in 0.1 mL saline was injected via the tail vein. 2, 10, 30, 60 min post-injection, mice were sacrificed by decapitation and interested organs were collected, weighted in pre-weighed plastic bags. The gall bladders were not included with the livers, and the pancreases were separated from the intestines. The whole tails were also measured and deducted to determine the total activities that entered the circulation. Activities in organs were measured by a WIZARD^2 2480 automatic γ-counter (Perkin Elmer, USA, ~70% efficiency). 100 μL (same volume as injected) of 100 times dilution of the injected dose as 1 %ID was counted under the same treatment. The uptake in organs was expressed as the percentage of the injected dose per gram organ (%ID/g) calculated as the ratio of count per minute (cpm).

microPET-CT imaging with an AD transgenic model

1.85 ± 0.50 MBq [^{18}F]**12** in 100 μL saline containing 5% ethonal were injected into 7-month

old 5×FAD mice (male, 22-26 g) via the caudal lateral tail vein. 20 min post injection, mice were anesthetized using isoflurane (delivered as a gas mixed with air, 2.5% isoflurane for preparation and 1.5% during scan) and placed on the bed of microPET-CT machine (Siemens, Inveon). 30 min post injection, a static scan was acquired for 5 minutes while the animal was kept warm by a heated pad on the scanner bed. A baseline low-dose CT scan was then obtained for localization and attenuation correction. PET images were reconstructed by a 2D OSEM/MAP reconstruction algorithm by the Inveon Acquisition Workplace Software (Siemens, Germany). [^{18}F]**2** (injected dose 1.85 ± 0.50 MBq), [^{18}F]FDG (injected dose 3.7 ± 0.5 MBq) were also injected in the tail vein of 5×FAD or normal mice. Images were acquisitioned under same treatment for comparison.

Acknowledgements

This work was funded by National Natural Science Foundation of China (81501534, 21271030, 81471707, 81402648 and 81200991), National Key Basic Research Program of China (2014CB744503) and Young and Middle-aged Talent Training Key Project in Health System of Fujian Province (2014-ZQN-ZD-11). The authors declare no competing financial interest.

We thank Prof. Huabei Zhang (College of Chemistry, Beijing Normal University) for assistance in the molecular docking.

Supporting Information Available: characterization of the precursor and reference compounds, purity of newly synthesized compounds, stability study of [^{18}F]**12**, standard curve of UV absorption of compound **12**, preparation and quality control data of [^{18}F]AV-45,

whole body microPET/CT imaging, Molecular Formula Strings Spreadsheet.

Corresponding Authors:

Dr. Zijing Li, zijing.li@xmu.edu.cn, +86-592-2880643

Dr. Xiaodong Pan, pxd77316@163.com, +86-591-83357896-8035

Dr. Xianzhong Zhang, zhangxzh@xmu.edu.cn, +86-592-2880645

References

1. Stern, Y. Cognitive reserve in ageing and Alzheimer's disease. *Lancet Neurol.* **2012**, *11*, 1006-1012.

2. Ryman, D. C.; Acosta-Baena, N.; Aisen, P. S.; Bird, T.; Danek, A.; Fox, N. C.; Goate, A.; Frommelt, P.; Ghetti, B.; Langbaum, J. B.; Lopera, F.; Martins, R.; Masters, C. L.; Mayeux, R. P.; McDade, E.; Moreno, S.; Reiman, E. M.; Ringman, J. M.; Salloway, S.; Schofield, P. R.; Sperling, R.; Tariot, P. N.; Xiong, C.; Morris, J. C.; Bateman, R. J.; Dominantly Inherited Alzheimer, N. Symptom onset in autosomal dominant Alzheimer disease: a systematic review and meta-analysis. *Neurology* **2014**, *83*, 253-260.

3. Dubois, B.; Hampel, H.; Feldman, H. H.; Scheltens, P.; Aisen, P.; Andrieu, S.; Bakardjian, H.; Benali, H.; Bertram, L.; Blennow, K.; Broich, K.; Cavedo, E.; Crutch, S.; Dartigues, J. F.; Duyckaerts, C.; Epelbaum, S.; Frisoni, G. B.; Gauthier, S.; Genthon, R.; Gouw, A. A.; Habert, M. O.; Holtzman, D. M.; Kivipelto, M.; Lista, S.; Molinuevo, J. L.; O'Bryant, S. E.; Rabinovici, G. D.; Rowe, C.; Salloway, S.; Schneider, L. S.; Sperling, R.; Teichmann, M.; Carrillo, M. C.; Cummings, J.; Jack, C. R., Jr.; Proceedings of the Meeting of the International Working Group (IWG) and the American Alzheimer's Association on

"The Preclinical State of A D; July 23, 2015; Washington DC, U. S. A. Preclinical Alzheimer's disease: Definition, natural history, and diagnostic criteria. *Alzheimer's Dement.* **2016**, *12*, 292-323.

4. Ballatore, C.; Lee, V. M.; Trojanowski, J. Q. Tau-mediated neurodegeneration in Alzheimer's disease and related disorders. *Nat. Rev. Neurosci.* **2007**, *8*, 663-672.

5. Krstic, D.; Knuesel, I. Deciphering the mechanism underlying late-onset Alzheimer disease. *Nat. Rev. Neurol.* **2013**, *9*, 25-34.

6. Heneka, M. T.; Golenbock, D. T.; Latz, E. Innate immunity in Alzheimer's disease. *Nat. Immunol.* **2015**, *16*, 229-236.

7. Petersen, R. C.; Caracciolo, B.; Brayne, C.; Gauthier, S.; Jelic, V.; Fratiglioni, L. Mild cognitive impairment: a concept in evolution. *J. Intern. Med.* **2014,** *275*, 214-228.

8. (a) Zhu, L.; Ploessl, K.; Kung, H. F. PET/SPECT imaging agents for neurodegenerative diseases. *Chem. Soc. Rev.* **2014**, *43*, 6683-6691; (b) Staderini, M.; Martin, M. A.; Bolognesi, M. L.; Menendez, J. C. Imaging of beta-amyloid plaques by near infrared fluorescent tracers: a new frontier for chemical neuroscience. *Chem. Soc. Rev.* **2015**, *44*, 1807-1819.

9. (a) Rowe, C. C.; Villemagne, V. L. Brain amyloid imaging. *J. Nucl. Med.* **2011**, *52*, 1733-1740; (b) Vallabhajosula, S. Positron emission tomography radiopharmaceuticals for imaging brain Beta-amyloid. *Semin. Nucl. Med.* **2011**, *41*, 283-299; (c) Nagren, K.; Halldin, C.; Rinne, J. O. Radiopharmaceuticals for positron emission tomography investigations of Alzheimer's disease. *Eur. J. Nucl. Med. Mol.* **2010**, *37*, 1575-1593; (d) Marc, L.; Slifstein. M.; Huang, Y. Relationships between radiotracer properties and image quality in molecular imaging of the brain with positron emission tomography. *Mol. Imaging Biol.* **2003**, *5*,

363-375; (e) Morais, G. Paulo, A.; Santos, I. A synthetic overview of radiolabeled compounds for β-amyloid targeting. *Eur. J. Org. Chem.* **2012**, *2012*, 1279-1293.

10. Ono, M. Development of positron-emission tomography/single-photon emission computed tomography imaging probes for in vivo detection of beta-amyloid plaques in alzheimer's brains. *Chem. Pharm. Bull.* **2009**, *57*, 1029-1039.

11. Wu, C.; Bowers, M. T.; Shea, J. E. On the origin of the stronger binding of PIB over thioflavin T to protofibrils of the Alzheimer amyloid-beta peptide: a molecular dynamics study. *Biophys. J.* **2011**, *100*, 1316-1324.

12. (a) Duara, R.; Loewenstein, D. A.; Shen, Q.; Barker, W.; Potter, E.; Varon, D.; Heurlin, K.; Vandenberghe, R.; Buckley, C. Amyloid positron emission tomography with ^{18}F-flutemetamol and structural magnetic resonance imaging in the classification of mild cognitive impairment and Alzheimer's disease. *Alzheimer's Dement.* **2013**, *9*, 295-301; (b) Vandenberghe, R.; Van Laere, K.; Ivanoiu, A.; Salmon, E.; Bastin, C.; Triau, E.; Hasselbalch, S.; Law, I.; Andersen, A.; Korner, A.; Minthon, L.; Garraux, G.; Nelissen, N.; Bormans, G.; Buckley, C.; Owenius, R.; Thurfjell, L.; Farrar, G.; Brooks, D. J. ^{18}F-flutemetamol amyloid imaging in Alzheimer disease and mild cognitive impairment: a phase 2 trial. *Ann. Neurol.* **2010**, *68*, 319-329.

13. (a) Choi, S. R.; Golding, G.; Zhuang, Z.; Zhang, W.; Lim, N.; Hefti, F.; Benedum, T. E.; Kilbourn, M. R.; Skovronsky, D.; Kung, H. F. Preclinical properties of ^{18}F-2: a PET agent for Abeta plaques in the brain. *J. Nucl. Med.* **2009**, *50*, 1887-1894; (b) Wong, D. F.; Rosenberg, P. B.; Zhou, Y.; Kumar, A.; Raymont, V.; Ravert, H. T.; Dannals, R. F.; Nandi, A.; Brasic, J. R.; Ye, W.; Hilton, J.; Lyketsos, C.; Kung, H. F.; Joshi, A. D.; Skovronsky, D. M.; Pontecorvo, M.

J. In vivo imaging of amyloid deposition in Alzheimer disease using the radioligand ^{18}F-AV-45 (Florbetapir F 18). *J. Nucl. Med.* **2010**, *51*, 913-920.

14. Verhoeff, N. P.; Wilson, A. A.; Takeshita, S.; Trop, L.; Hussey, D.; Singh, K.; Kung, H. F.; Kung, M. P.; Houle, S. In-vivo imaging of Alzheimer disease beta-amyloid with [^{11}C]SB-13 PET. *Am. J. Geriatr. Psychiatry* **2004**, *12*, 584-595.

15. (a) Rowe, C. C.; Ng, S.; Ackermann, U.; Gong, S. J.; Pike, K.; Savage, G.; Cowie, T. F.; Dickinson, K. L.; Maruff, P.; Darby, D.; Smith, C.; Woodward, M.; Merory, J.; Tochon-Danguy, H.; O'Keefe, G.; Klunk, W. E.; Mathis, C. A.; Price, J. C.; Masters, C. L.; Villemagne, V. L. Imaging beta-amyloid burden in aging and dementia. *Neurology* **2007**, *68*, 1718-1725; (b) Linazasoro, G. Imaging beta-amyloid burden in aging and dementia. *Neurology* **2008**, *70*, 1649.

16. (a) Yang, Y.; Cui, M.; Zhang, X.; Dai, J.; Zhang, Z.; Lin, C.; Guo, Y.; Liu, B. Radioiodinated benzyloxybenzene derivatives: a class of flexible ligands target to beta-amyloid plaques in Alzheimer's brains. *J. Med. Chem.* **2014**, *57*, 6030-6042; (b) Yang, Y.; Zhang, X.; Cui, M.; Zhang, J.; Guo, Z.; Li, Y.; Zhang, X.; Dai, J.; Liu, B. Preliminary characterization and in vivo studies of structurally identical ^{18}F- and ^{125}I-labeled benzyloxybenzenes for pet/spect imaging of beta-amyloid plaques. *Sci. Rep.* **2015**, *5*, 12084.

17. Kung, M. P.; Hou, C.; Zhuang, Z. P.; Zhang, B.; Skovronsky, D.; Trojanowski, J. Q.; Lee, V. M.; Kung, H. F. 1: an improved thioflavin-T derivative for in vivo labeling of beta-amyloid plaques. *Brain Res.* **2002**, *956*, 202-210.

18. Jin, G.; Wong, S. T. Toward better drug repositioning: prioritizing and integrating existing methods into efficient pipelines. *Drug Discovery Today* **2014**, *19*, 637-644.

19. Ernest R. Davidson, D. F. Basis set selection for molecular calculations. *Chem. Rev.* **1986**, *86*, 681-696.

20. Petkova, A. T.; Yau, W. M.; Tycko, R. Experimental constraints on quaternary structure in Alzheimer's beta-amyloid fibrils. *Biochemistry* **2006**, *45*, 498-512.

21. Tong, H.; Lou, K.; Wang, W. Near-infrared fluorescent probes for imaging of amyloid plaques in Alzheimers disease. *Acta Pharm. Sin. B* **2015**, *5*, 25-33.

22. Wilson, A. A., Jin, L., Garcia, A., DaSilva, J.N., Houle, S. An admonition when measuring the lipophilicity of radiotracers using counting techniques. *Appl. Radiat. Isot.* **2001**, *54*, 203-208.

23. (a) Jawhar, S.; Trawicka, A.; Jenneckens, C.; Bayer, T. A.; Wirths, O. Motor deficits, neuron loss, and reduced anxiety coinciding with axonal degeneration and intraneuronal Abeta aggregation in the 5XFAD mouse model of Alzheimer's disease. *Neurobiol. Aging* **2012**, *33*, 196 e29-40; (b) Kimura, R.; Ohno, M. Impairments in remote memory stabilization precede hippocampal synaptic and cognitive failures in 5XFAD Alzheimer mouse model. *Neurobiol. Dis.* **2009**, *33*, 229-235; (c) Oakley, H.; Cole, S. L.; Logan, S.; Maus, E.; Shao, P.; Craft, J.; Guillozet-Bongaarts, A.; Ohno, M.; Disterhoft, J.; Van Eldik, L.; Berry, R.; Vassar, R. Intraneuronal beta-amyloid aggregates, neurodegeneration, and neuron loss in transgenic mice with five familial Alzheimer's disease mutations: potential factors in amyloid plaque formation. *J. Neurosci.* **2006**, *26*, 10129-10140.

24. Zeng, Y.; Zhang, J.; Zhu, Y.; Zhang, J.; Shen, H.; Lu, J.; Pan, X.; Lin, N.; Dai, X.; Zhou, M.; Chen, X. Tripchlorolide improves cognitive deficits by reducing amyloid beta and upregulating synapse-related proteins in a transgenic model of Alzheimer's Disease. *J.*

Neurochem. **2015**, *133*, 38-52.

25. Rowe, C. C.; Pejoska, S.; Mulligan, R. S.; Jones, G.; Chan, J. G.; Svensson, S.; Cselenyi, Z.; Masters, C. L.; Villemagne, V. L. Head-to-head comparison of ^{11}C-PiB and 18F-AZD4694 (NAV4694) for beta-amyloid imaging in aging and dementia. *J. Nucl. Med.* **2013**, *54*, 880-886.

26. Li, Z. J.; Cui, M. C.; Zhang, J. M.; Dai, J. P.; Zhang, X. J.; Chen, P.; Jia, H. M.; Liu, B. L. Novel F-18-labeled dibenzylideneacetone derivatives as potential positron emission tomography probes for in vivo imaging of beta-amyloid plaques. *Eur. J. Med. Chem.* **2014**, *84*, 628-638.

27. Handoko, S. D.; Ouyang, X.; Su, C. T.; Kwoh, C. K.; Ong, Y. S. QuickVina: accelerating AutoDock Vina using gradient-based heuristics for global optimization. *IEEE/ACM Trans. Comput. Biol. Bioinform.* **2012**, *9*, 1266-1272.

Table of Contents graphic